### JPhys Energy

#### **PAPER • OPEN ACCESS**

# Enhanced metal exsolution at the non-polar (001) surfaces of multi-faceted epitaxial thin films

To cite this article: Moritz L Weber et al 2023 J. Phys. Energy 5 014002

View the article online for updates and enhancements.

#### You may also like

Tracking the Nanoparticle
 Exsolution/Reoxidation Process in Ni Doped SrTi<sub>0.3</sub>Fe<sub>0.7</sub>O<sub>3</sub>. Electrodes for Intermediate Temperature Symmetric SOFC

Mariano Santaya, Catalina Elena Jiménez, Mauricio D. Arce et al.

- A-site deficient La<sub>0.52</sub>Sr<sub>0.22</sub>Ti<sub>0.94</sub>Ni<sub>0.06</sub>O<sub>3</sub> by low-pulsed electric current treatment: achieved exsolution of B-site Ni nanoparticles and significant improvement of electrocatalytic properties
   Wenwen Yu, Jingang Qi, Xin Hu et al.
- Rapid and Efficient Exsolution of Nanoparticles in Perovskites Oxides By Atmospheric-Pressure Plasma Atta ul HAQ, Fiorenza Fanelli, Hessan Khalid et al.

### Journal of Physics: Energy



#### **OPEN ACCESS**

#### RECEIVED

23 July 2022

REVISED

14 October 2022

ACCEPTED FOR PUBLICATION 26 October 2022

PUBLISHED

21 November 2022

Original content from this work may be used under the terms of the Creative Commons Attribution 4.0 licence.

Any further distribution of this work must maintain attribution to the author(s) and the title of the work, journal citation and DOI.



#### **PAPER**

# Enhanced metal exsolution at the non-polar (001) surfaces of multi-faceted epitaxial thin films

Moritz L Weber<sup>1,2,3,9,\*</sup>, Moritz Kindelmann<sup>2,4</sup>, Egbert Wessel<sup>5</sup>, Alexandros Sarantopoulos<sup>1,3</sup>, Norbert H Menzler<sup>2,6</sup>, Regina Dittmann<sup>1,3</sup>, Rainer Waser<sup>1,3,7</sup>, Olivier Guillon<sup>2,6,8</sup>, Christian Lenser<sup>2,\*</sup> and Felix Gunkel<sup>1,3,\*</sup>

- <sup>1</sup> Peter Gruenberg Institute (PGI-7), Forschungszentrum Juelich GmbH, D-52425 Juelich GmbH, Germany
- <sup>2</sup> IEK-1, Forschungszentrum Juelich GmbH, D-52425 Juelich, Germany
- Juelich-Aachen Research Alliance (JARA-FIT), D-52425 Juelich, Germany
- <sup>4</sup> ER-C, Forschungszentrum Juelich GmbH, D-52425 Juelich, Germany
- <sup>5</sup> IEK-2, Forschungszentrum Juelich GmbH, D-52425 Juelich, Germany
- <sup>6</sup> RWTH Aachen University, Institute of Mineral Engineering, 52074 Aachen, Germany
- Institute for Electronic Materials (IWE 2), RWTH Aachen University, D-52074 Aachen, Germany
- <sup>8</sup> Juelich Aachen Research Alliance (JARA-Energy), 52425 Juelich, Germany
- Present address: Advanced Light Source, Lawrence Berkeley National Laboratory, Berkeley, CA 94720, United States of America.
- \* Authors to whom any correspondence should be addressed.

E-mail: mo.weber@fz-juelich.de, c.lenser@fz-juelich.de and f.gunkel@fz-juelich.de

**Keywords:** metal exsolution, nanoparticles, catalysis, surface orientation, epitaxy, surface reconstruction Supplementary material for this article is available online

#### **Abstract**

Metal exsolution is a dynamic process driven under a reducing atmosphere and at elevated temperatures that results in the self-assembly of nanoparticles at the surface of complex perovskite catalysts. The nanoparticle characteristics of metal exsolution catalysts can be subject to considerable inhomogeneity, and the anisotropic surface properties of ceramic oxides have been identified to have a major influence on the exsolution behavior. We systematically reveal the orientation-dependent anisotropy of the exsolution behavior of Ni in SrTi<sub>0.9</sub>Nb<sub>0.05</sub>Ni<sub>0.05</sub>O<sub>3-δ</sub> using multi-faceted epitaxial thin films that represent a material system with properties in between functional ceramics and single-crystalline perovskite thin film model systems. Using an approach of combined orientation mapping and surface imaging we study the exsolution behavior with particular focus on the initial exsolution response, i.e. after short annealing times. We find orientation-specific variations in the surface morphology of the thin film facets. In the as-prepared state, surface reconstructions cause the formation of patterned surface structures for all thin film facets apart from (001) surfaces, which exhibit a plain surface morphology as well as an enhanced exsolution response. Surface reconstructions and their inherent energy landscape may hence cause an additional energy barrier for the exsolution reaction that results in orientation-dependent differences in the exsolution kinetics.

#### 1. Introduction

Metal exsolution allows for the fabrication of supported nanoparticles by the precipitation of dopants that are released from a perovskite host oxide under reducing conditions. The product is a nanostructured metal—oxide composite with catalytic functionality with applications, for example, in solid oxide cells, where exsolution-active perovskites can be applied for the design of high-performance fuel electrodes [1–3]. The exsolution process, and therefore the nanoparticle properties, are influenced by interactions between the exsolving species and the oxide host lattice. For instance, the exsolution behavior has been demonstrated to depend on stoichiometric and structural effects, namely the defect structure of the perovskite parent oxide as well as related parameters such as lattice strain that may dynamically change over the course of the reduction process [4–7].

Furthermore, the characteristics of the exsolved metal nanoparticles have been shown to depend on the crystallographic orientation of the oxide support [6, 8–10]. Here, orientation-dependent exsolution in perovskites was discussed with respect to differences in the atomic (defect) composition of the termination plane [10] and the influence of extended surface reconstruction layers [6], the surface roughness [10] as well as the ion surface diffusivity and particle mobility, that was shown to be influenced by the interfacial energy and the relationship of structural orientation between the nanoparticles and the oxide support [8, 9]. As a consequence, considerable inhomogeneities in the nanoparticle characteristics can be expected for technically relevant porous ceramics with a large variety of surface orientations of the oxide grains that form the electrochemical interface due to differences in the extent of nanoparticle embedment, the kinetics of nanoparticle growth and, ultimately, differences in the stability of the supported nanoparticles [8, 9]. Since the nanoparticle properties and particle distribution at the perovskite surface can be expected to have a considerable influence on the catalytic performance, a detailed understanding of the processes that are involved in nanoparticle nucleation and self-assembly during metal exsolution is required.

Epitaxial thin films can be employed as useful model systems for investigating the metal exsolution behavior at well-defined surfaces [5, 7–9, 11] since epitaxial growth allows for the systematic control of their structural properties such as crystallographic orientation [8, 9]. In the present study, we demonstrate that the reconstruction of polar perovskite surfaces may influence the exsolution behavior contributing to the anisotropic non-uniform growth of Ni nanoparticles during metal exsolution at differently oriented facets of  $SrTi_{0.9}Nb_{0.05}Ni_{0.05}O_{3-\delta}$  (STNNi), with particular focus on the initial exsolution response. For this purpose, we employ epitaxial thin films that are deposited on polished polycrystalline  $SrTiO_{3-\delta}$  (pc-STO) substrates to mimic the multi-faceted morphology of oxide ceramics. Our approach allows us to study the exsolution behavior at STNNi facets of different orientation, including high-index planes, where we find considerable differences in the nanoparticle properties even for minor differences in the orientation of the parent oxide grains. In particular, we observe an enhanced exsolution response at the (001) facets of STNNi relative to grains of other surface orientations, which is associated with early particle formation and, ultimately, a greater nanoparticle height. We show that surface reconstructions that are energetically favorable for polar perovskite surfaces and visible in form of patterned surface structures may cause a more sluggish mass transfer of Ni to the surface. Our observations indicate that to understand the origin of variations in the properties of exsolved nanoparticles we need to consider not only the growth kinetics of the nanoparticles at the oxide surface but also the dynamics of the mass transfer of exsolution-active species from the near-surface region of the oxide to the solid–gas interface.

#### 2. Method

Polycrystalline STO substrates were fabricated by cutting discs approximately 2 mm thick and 1 cm in diameter from a ceramic pellet prepared from STO powder that was synthesized by the Pechini method. After initial polishing of the substrate surface with SiC paper and diamond suspension a final polishing step was performed using a SiO<sub>2</sub> suspension (50 nm). Subsequently high-temperature heat treatment under continuous flow of an Ar/O<sub>2</sub> gas mixture (80:20) was carried out at  $T=1000\,^{\circ}\mathrm{C}$  for  $t=2\,\mathrm{h}$  to obtain smooth surface facets. For convenient localization of the probing area, each of the pc-STO substrates was indented using a Vickers hardness testing machine in order to mark a specific sample region, as demonstrated in [12, 13], for correlated analyses of the surface orientation and the surface morphology. Epitaxial growth of 50 nm thick thin films was performed by pulsed laser deposition (PLD), where the growth rate was calibrated by *in situ* monitoring of the growth of STNNi on a (001) single-crystalline STO substrate using reflection high-energy electron diffraction. PLD was performed with a KrF excimer laser with a wavelength of  $\lambda=248\,\mathrm{nm}$  using a repetition rate of  $f=5\,\mathrm{Hz}$ , a laser fluence of  $F=1.14\,\mathrm{J}$  cm<sup>-2</sup>, a substrate temperature of  $T=650\,^{\circ}\mathrm{C}$  and an oxygen background pressure of  $p(\mathrm{O}_2)=0.108\,\mathrm{mbar}$ . The target-to-substrate distance was  $d=60\,\mathrm{mm}$ . The sample temperature was quenched to room temperature after completion of the thin film growth.

Scanning electron microscopy (SEM; Zeiss Merlin) was performed using an acceleration voltage between 10 and 20 keV after deposition of a thin conductive carbon layer. The crystallographic orientation of the perovskite facets of substrates and epitaxial thin films was investigated by recording orientation maps by electron backscatter diffraction (EBSD; Oxford Instruments). The Euler angle is directly accessible as a result of the EBSD measurements. Notably, the surface exsolution response was exclusively investigated by employing thin films that had not been coated with carbon, where the orientation of the oxide facets was determined by analysis of the respective substrate prior to the epitaxial growth.

Atomic force microscopy (AFM; Cypher, Oxford Instruments Asylum Research Inc.) was carried out in tapping mode. Evaluation of the surface roughness and nanoparticle properties was performed on the basis of the topological data obtained by AFM using Gwyddion 2.52. The average surface roughness was

determined based on three measurements at different locations on each facet. The average nanoparticle height was determined on the basis of three particles per facet. For this purpose, the surface was leveled in the direct vicinity of each particle using the three-point leveling tool and the minimum height was set to zero right next to the bottom of each nanoparticle. The error bars denote the standard deviation of the average value determined from the measurements of three nanoparticles. Notably the curvature of the thin film facets prevents automated evaluation of the topological data with respect to the entire nanoparticle population with improved statistics that can be typically employed for epitaxial thin films that are deposited on single-crystal substrates. To improve the visibility, a polynomial background (second degree) was subtracted for the AFM images shown in figure 2 instead of using the median.

The crystallographic properties of the pc-STO substrates and epitaxial STNNi thin films were investigated by x-ray diffraction analysis in grazing incidence measurement geometry (D8 Discover, Bruker AXS GmbH). Metal exsolution was induced by thermal annealing treatment under continuous flow of a 4%  $H_2$ /Ar gas mixture at different temperatures of T = 500 °C, 600 °C and 700 °C, and subsequently the sample was quenched to room temperature.

#### 3. Results

AFM revealed a smooth surface morphology of the pc-STO substrates (figure S1). The average surface roughness locally determined for various individual oxide grains was RMS =  $435 \pm 125$  pm, comparable to the roughness of single-crystalline substrates and well suited for the deposition of epitaxial thin films.

Since nucleation during PLD typically takes place on the length scale of atomic step terraces (i.e. <200 nm), the grains of the pc-STO substrate are comparably large to allow epitaxial growth of STNNi on each individual surface facet of the substrate. Therefore, the STNNi thin film adapts the morphology and crystallographic orientation of the respective underlying substrate grain that serves as a nucleation template, resulting in the deposition of a multi-faceted thin film (figure 1(a)) with well-comparable frequency distribution of the grain size and the surface orientation (cf figure S2). This result indicates that each individual grain should comprise an epitaxial relationship between substrate and thin film. The growth parameters were optimized with respect to stoichiometry based on (001) SrTiO<sub>3</sub> single-crystal substrate epitaxy as described in detail in [7], resulting in a continuous layer-by-layer growth mode. Grazing incidence x-ray diffraction analysis confirms that the substrate and thin film crystallize in the perovskite structure (figure 1(b)). Additionally, a minor secondary phase is detected only for the substrate, which is likely to originate from a TiO<sub>2</sub> anatase impurity [14], consistent with energy-dispersive x-ray spectroscopy measurements that revealed a minor, sparsely distributed Ti-rich secondary phase (figure S3). No TiO<sub>2</sub> phase was detected after thin film deposition, which may confirm homogeneous epitaxial growth of STNNi on each grain of the pc-STO substrate. SEM was carried out to investigate the surface morphology of the multi-faceted (mf-STNNi) thin film while EBSD was applied to study the crystallographic orientation of the surface facets. SEM imaging revealed considerable differences in the surface morphology of the different perovskite facets; while certain facets have a plain appearance most of the oxide surfaces exhibit a distinctly patterned surface morphology (figure 1(c)). Importantly, similar differences in the surface morphology of different perovskite grains are also visible for the as-prepared pc-STO substrates (cf figure S1). The orientation map given in figure 1(d) shows the surface orientation in the sample normal direction  $(z_0)$ . Based on the EBSD mapping it becomes apparent that the plain surface morphologies are solely found for (001) perovskite facets, while a deviation from the ideal (001) surface orientation results in the formation of a patterned surface structure. The apparent difference in the surface morphology of different thin film facets is most likely related to polarity-driven reconstructions of perovskite surfaces of a certain orientation [15]. Here, the surface polarity results from the dipole moment perpendicular to the surface, which is associated with the stacking sequence of the atomic planes.

While STO (101) surfaces with a stacking sequence of  $(SrTiO)^{4+}$ – $(O_2)^{4-}$  as well as STO (111) surfaces with a stacking sequence of  $(SrO_3)^{4-}$ – $(Ti)^{4+}$  are polar, the STO (001) surface with a stacking sequence of (SrO)– $(TiO_2)$  may be considered non-polar. As a consequence of polarity, the surface energy of extended grains becomes infinite, causing inherent instability of polar surfaces [15, 16]. Therefore, the charge at the (101) and (111) surface needs to be compensated either electronically or by changes in the chemical and structural composition of the surface [17–19]. The observation of orientation-dependent differences in the surface morphology may therefore be related to chemical, electronic and structural reconstructions, which may affect the exsolution behavior.

In order to investigate the initial exsolution response at thin film facets of various surface orientations and surface morphologies, the pc-STO substrates were indented prior to thin film growth to mark a region of the thin film for convenient localization of the probing area (figure S4), as demonstrated in [12, 13]. Here, the characteristic grain boundary pattern of the surface serves as a fingerprint to identify the grains and to

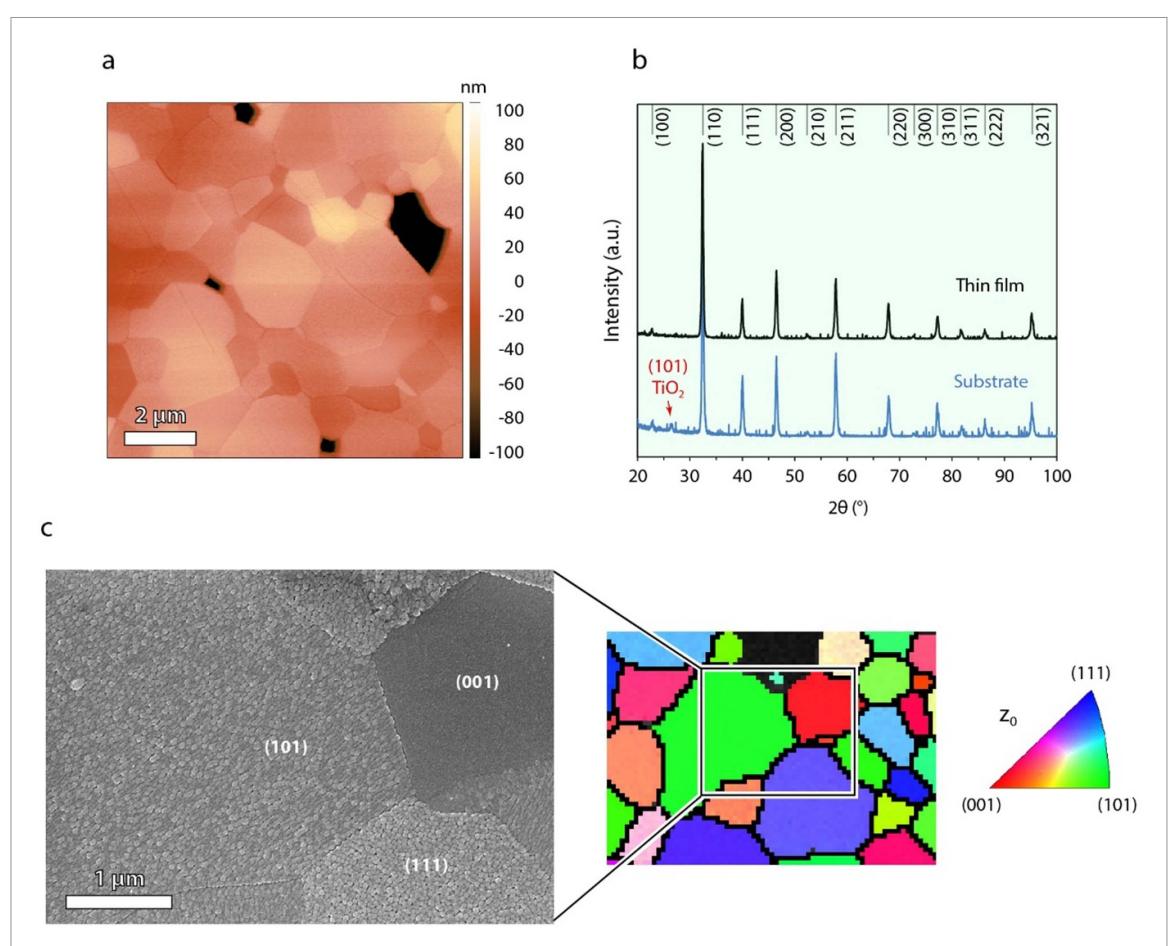


**Figure 1.** Characterization of a representative 50 nm thick as-prepared STNNi thin film deposited on a polished pc-SrTiO<sub>3</sub> substrate. (a) Representative AFM image of the multi-faceted thin film surface in the as-prepared state. (b) X-ray diffractogram of a pc-STO substrate (blue) and a mf-STNNi thin film (black) obtained in grazing incidence measurement geometry. (c) SEM-EBSD analysis reveals differences in the surface morphology of perovskite facets with different orientations. Perovskite facets in (001) orientation exhibit a plain surface morphology, while facets in other orientations exhibit a patterned surface structure. Before imaging, the thin film was coated with a thin layer of carbon.

assign the surface morphology to the respective facet of the crystal. Figure 2 shows the surface morphology of mf-STNNi thin films after heat treatment in a reducing atmosphere (4% H<sub>2</sub>/Ar) at different temperatures of T = 500 °C, 600 °C and 700 °C for t = 1 h, respectively (figure 2(b)). The surface orientation map of the respective imaging area is shown in figure 2(a), allowing for a convenient assignment of the facet morphology to the crystallographic orientation (full EBSD maps are shown in figures S5–S7). As can be seen, no considerable changes in the surface morphology can be observed on this time scale after a reducing treatment at T = 500 °C, while after thermal reduction of the samples at T = 600 °C distinct changes in the surface morphology are visible for certain facets of the thin film, where surface decoration and the early stages of nanoparticle formation can be observed. Based on the orientation maps it becomes apparent that this early exsolution response is only visible for the (001) facets of the mf-STNNi thin films. In comparison, widespread formation of exsolution nanoparticles is visible among perovskite facets of various surface orientations only at increased annealing temperatures of T = 700 °C. The difference in the early exsolution response is further illustrated in figure 2(c), showing the change in the average surface roughness as a function of the annealing temperature for surfaces of low-index (001), (101) and (111) facets. Here, the surface roughness may serve as a parameter for the beginning of the exsolution reaction to qualitatively evaluate the early stages of metal exsolution, since the detection of distinct nanoparticles is difficult. After annealing at T = 500 °C, the surface roughness of all facets remains similar. Consistent with the visible changes in figure 2(b), reducing annealing at T = 600 °C results in a strong change in the average surface roughness for (001) facets, while no statistically significant changes can be observed for the (101) and (111) facets, which show a considerable increase in surface roughness only after annealing at higher temperatures of T = 700 °C.

On the investigated time scale, orientation-dependent exsolution is apparent mainly at intermediate exsolution temperatures, diminishing at a higher applied temperature. This behavior hints at a kinetic

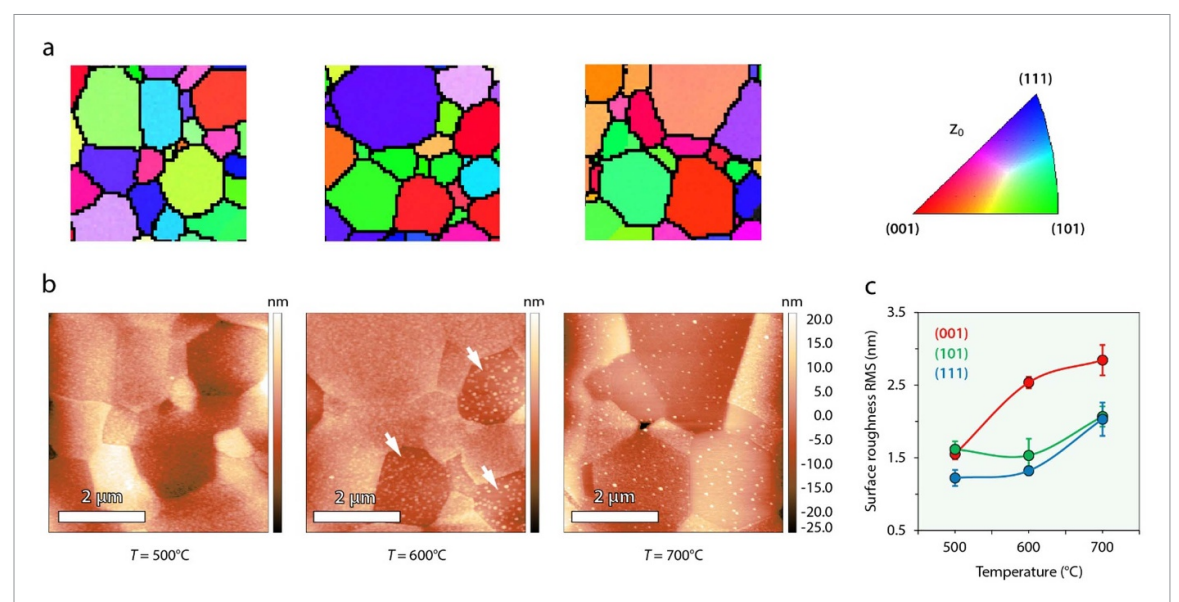


**Figure 2.** Imaging of the initial exsolution response at the surfaces of mf-STNNi thin films after thermal reduction at different temperatures of  $T = 500 \,^{\circ}$ C,  $600 \,^{\circ}$ C and  $700 \,^{\circ}$ C for 1 h, respectively (4% H<sub>2</sub>/Ar). Combined (a) EBSD orientation mapping (of the substrate) and (b) AFM analysis is performed to investigate differences in the initial nanoparticle growth at thin film facets of various surface orientations under the same conditions. (c) The surface roughness obtained from (001), (101) and (111) facets after the thermal reduction treatment. After reducing annealing at  $T = 600 \,^{\circ}$ C, early metal exsolution can be observed by AFM imaging for (001) facets (highlighted by white arrows) and from the increased surface roughness in (c).

phenomenon that becomes insignificant at increasing temperatures. These observations presumably indicate a difference in the energy barrier for the exsolubility of Ni at surface facets of different orientation that may cause a difference in the mass transfer dynamics of the exsolution-active species to the solid—gas interface. Orientation-dependent mass transfer dynamics are expected to influence the kinetics of nanoparticle formation and, in consequence, the nanoparticle characteristics such as size and distribution. So far mostly processes subsequent to the exsolution reaction, for example surface diffusion and coalescence, have been considered to play a major role in this regard [8, 9]. However, the specific nanoparticle size distribution and coverage of the product is likely to be determined by different interrelated processes, including the mass transfer to the solid—gas interface and subsequent surface diffusion and nucleation at the surface, causing considerable local differences in the nanoparticle properties according to differences in the dynamics of these processes, particularly for short annealing times.

In order to evaluate the influence of the enhanced exsolution dynamics at the (001) STNNi facets on nanoparticle formation, the average maximum nanoparticle height of the exsolved nanoparticles was analyzed for various facets after thermal reduction at  $T=700\,^{\circ}$ C. In figure 3 the maximum nanoparticle height is plotted as a function of the Euler angle that is determined by EBSD orientation mapping and can serve as a parameter that indicates small differences in the surface orientation of the thin film facets. Additionally, data points that can be assigned to the low-index surface orientations (001), (011) and (111) are highlighted in red, green and blue, respectively. Surfaces that cannot be assigned to the latter low-index orientations are broadly summarized as high-index surfaces (open symbols). As can be seen, a strong influence of the surface orientation of the nanoparticle height becomes apparent. Here, low Euler angles, representing surface facets close to the (001) orientation, are associated with a larger nanoparticle height relative to nanoparticles that are exsolved at facets with larger Euler angles including the low-index (101) and (111) surfaces.

The investigation of the orientation-dependent exsolution response has been so far limited to low-index surfaces as the studies were based on commercially available single-crystal substrates. Employing multi-faceted thin films, however, additionally allows us to investigate the influence of small differences in the surface orientation on the nanoparticle growth at facets that would be nominally assigned to the (001) orientation as well as the exsolution behavior at high-index planes. As can be seen, even small differences in the surface orientation of (001) facets can result in clear changes in the nanoparticle height. Here, a systematic dependence between the nanoparticle height and incremental differences in the Euler angle of (001)-oriented surface facets can be observed ( $\Phi \sim 5^{\circ}-15^{\circ}$ ). In comparison, nanoparticles exsolved at high-index planes ( $\Phi \sim 15^{\circ}-40^{\circ}$ ) generally show a lower nanoparticle height, similar to (101) and (111) facets.

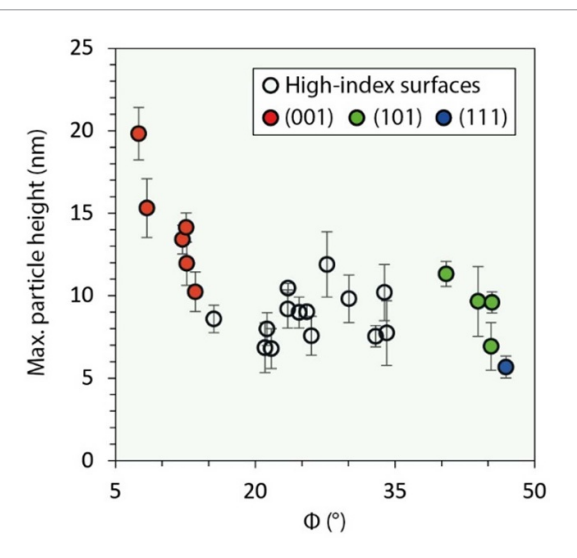
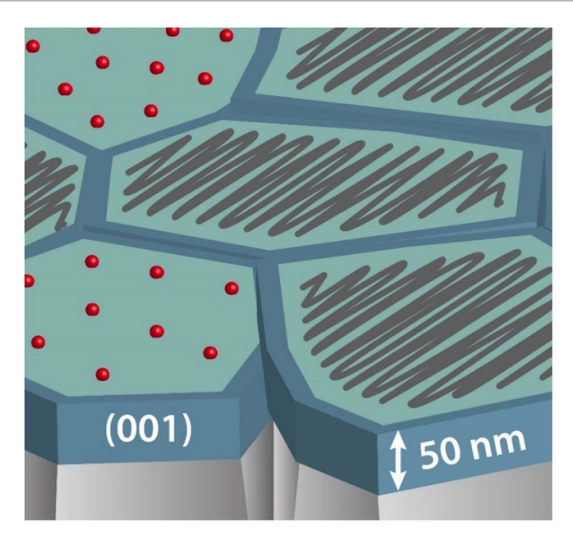


Figure 3. Evaluation of the maximum height of nanoparticles fabricated by metal exsolution at  $T=700\,^{\circ}\mathrm{C}$  ( $t=1\,\mathrm{h}$ , 4%  $\mathrm{H_2/Ar}$ ) with respect the surface orientation of the STNNi facets (Euler-angle  $\Phi$ ). The properties of three particles were analyzed for each facet; error bars denote the standard deviation of the measurements. For comparison red (001), green (101) and blue (111) symbols denote low-index planes. The exsolution response strongly depends on the surface orientation of the STNNi facets, where small differences in the orientation result in significant differences in the nanoparticle height.

#### 4. Discussion

Over the past decade, a large variety of material properties and parameters which influence metal exsolution reactions have been identified [20, 21]. Recent investigations of orientation-dependent metal exsolution behavior at perovskite surfaces offer variable and in part even contradictory findings. For instance, preferential exsolution was observed for the (001) facets of bulk ceramics (equal to (110) of the primitive SrTiO<sub>3</sub> unit cell as denoted in the original work) whereas metal exsolution was found to be suppressed for the other perovskite facets [10]. In contrast, studies that are based on single-crystal epitaxial thin film model systems have revealed the exsolution of nanoparticles at all low-index (001), (101) and (111) surfaces, but with considerable differences in the nanoparticle characteristics [8, 9]. Here the higher interfacial energy between the exsolved Ni nanoparticles and the (001) perovskite surface relative to the other surface orientations has been identified as the origin of the accelerated nanoparticle growth described by Kim et al [8]. It is worth pointing out that no considerable differences in the surface morphologies of the as-prepared epitaxial thin films with different crystallographic orientation were reported in that study. Interestingly, Jennings et al show that the smallest initial nanoparticle size can be detected at the (001) surface of Ni-doped  $BaZr_{0.9}Y_{0.1}O_{3-\delta}$  epitaxial thin films, which, however, exhibit the fastest coarsening dynamics during long-term reduction treatment [9]. As a result of the anisotropic coarsening dynamics during long-term reduction treatment, nanoparticles exsolving at the (111) surface exhibit an improved nanoparticle stability over time and a smaller nanoparticle size compared with nanoparticles that exsolve at the (001) and (101) surfaces [9], in line with the findings presented in [8]. The differences in the nanoparticle characteristics were found to be related to the anisotropic surface diffusivity as well as differences in the preferential orientation relationship between the metallic nanoparticles and the perovskite lattice for the different surface orientations that may be the predominant coarsening mechanisms [9].

Our study focuses on the initial exsolution response of Ni in STNNi after short annealing times. For this purpose, we demonstrate the synthesis of multi-faceted epitaxial thin films as a material system with properties in between single-crystal thin film model systems and technical ceramics, enabling the investigation of the orientation-dependent exsolution response over a large variety of surface orientations under defined exsolution conditions. Epitaxy of such multi-faceted thin films can help to close the gap between studies on single-crystal model systems and functional ceramics. Pronounced orientation-specific differences in the surface structure are apparent for the as-prepared thin film facets. Low-index (001) STNNi facets exhibit a plain surface morphology, while low-index (101) and (111) surfaces as well as high-index surfaces exhibit a patterned surface structure that point towards reconstructions of the termination layer induced during the high-temperature synthesis of perovskite oxide ceramics and thin films. Such surface reconstructions may be linked to compensation of the surface energy of polar surfaces. The nature of the surface morphology appears to influence the exsolution behavior. Here, an early exsolution response is



**Figure 4.** Schematic illustration of a multi-faceted epitaxial thin film deposited on a polished polycrystalline substrate. All surface facets apart from the (001) facets exhibit a patterned surface structure that presumably indicates the reconstruction of polar surfaces. The non-polar (001) facets show an enhanced exsolution response at lower temperatures compared with facets of other surface orientation that exhibit decreased exsolution kinetics.

apparent for non-polar (001) facets with initially plain surface morphology relative to patterned STNNi facets of various surface orientations (cf figure 4).

We propose that the reconstructed surface and its specific energy landscape may act as an additional energy barrier for the exsolution reaction. Therefore, our findings reveal a kinetic effect that comes into play during the initial stages of metal exsolution and may add to the complexity of anisotropic exsolution and nanoparticle formation dynamics, resulting in an enhanced exsolution response at (001) facets. Consistently, a larger average nanoparticle height is detected at (001) STNNi facets after reducing annealing at increased temperatures.

The effect may be associated with deviations in the surface defect structure that have been shown to play a major role in metal exsolution reactions. For example, defects that form during the synthesis of the parent perovskite or during reducing thermal annealing result in changes in the surface segregation energy [22] as well as in distinct electrostatic interactions between exsolving species and the surface potential that is formed as a consequence of space charge regions that are an inherent feature of oxide surfaces [23, 24].

Our observations are in line with experimental results obtained from ceramic oxides and with density functional theory calculations reporting on preferential exsolution at (001) surfaces [10, 22]. Moreover, our findings broadly support the exsolution trends that have been reported for single-crystalline epitaxial thin films, where the largest nanoparticle sizes were observed for (001)-oriented thin films, and decreasing nanoparticle dimensions were detected for (101) and (111) surfaces at the expense of larger nanoparticle densities [8, 9]. In addition, our approach allows us to study exsolution behavior at high-index surfaces, which exhibit a reconstructed surface structure similar to (101) and (111) facets, associated with a sluggish exsolution response. Consistently, nanoparticles that exsolve at high-index surfaces exhibit similar average heights to nanoparticles that are exsolved at (101) and (111) facets. Importantly, we observe a high sensitivity of the exsolution behavior of nanoparticles that exsolve at nominal (001) facets with respect to slight deviations from the ideal (001) surface orientation that are reflected by respective changes in the nanoparticle height.

While different parameters have been identified that may contribute to the anisotropic nanoparticle properties of metal exsolution catalysts, a universal understanding of the underlying processes is lacking. In particular, the interplay between different processes that are involved in nanoparticle formation during metal exsolution that typically proceed simultaneously during the self-assembly of nanoparticles at the solid–gas interface, for example mass transfer to the surface versus nucleation and particle growth, complicate the interpretation of metal exsolution behavior. Future research is required to clarify the mechanisms of interaction between exsolving species and the surface (defect) chemistry and the resulting electrostatic landscape of perovskite surfaces. Here, *in situ* analytical techniques may be of major importance to gain a detailed understanding of the structural and chemical evolution of exsolution catalysts over time and according on the processing or operation environment [25–27] in order to derive novel strategies for the control of the nanoparticle characteristics at perovskite catalysts that often exhibit a high degree of structural complexity.

#### 5. Conclusion

Since uniformity in dimensions as well as homogeneity in the density of exsolved nanoparticles will have a direct impact on the catalytic functionality of nanostructured exsolution catalysts, a detailed understanding of the anisotropic metal exsolution behavior at perovskite surfaces is crucial. Our study, which is based on multi-faceted epitaxial model systems, reveals a kinetic effect that results in differences in the metal exsolution dynamics at facets of different surface orientation during the initial exsolution response. The effect is presumably associated with orientation-specific surface reconstructions that may serve as an additional energy barrier for the exsolution reaction, where modifications in the chemical and structural properties or in the electrostatic potential at the surface of the perovskite grains are likely to play a role for the mass tranfer dynamics. Reconstructions are visible in the form of a distinct patterned surface morphology of perovskite facets of (101) and (111) orientation as well as for high-index surfaces, which exhibit a sluggish exsolution response relative to (001) surfaces. In contrast, the non-polar (001) facets exhibit a plain appearance which is correlated with enhanced exsolution dynamics. Our findings show that the orientation-specific exsolution dynamics may result in considerable differences in the nanoparticle characteristics at different facets even during the initial stages of the exsolution reaction, which in turn will influence the subsequent long-term evolution of the nanoparticle properties and catalytic activity.

#### Data availability statement

All data that support the findings of this study are included within the article (and any supplementary files).

#### ORCID iDs

Moritz L Weber https://orcid.org/0000-0003-1105-2474

Moritz Kindelmann https://orcid.org/0000-0001-9676-2090

Alexandros Sarantopoulos https://orcid.org/0000-0001-6988-0972

Norbert H Menzler https://orcid.org/0000-0001-7091-0980

Olivier Guillon https://orcid.org/0000-0003-4831-5725

Christian Lenser https://orcid.org/0000-0001-5636-2201

Felix Gunkel https://orcid.org/0000-0003-1178-9986

#### References

- [1] Tsekouras G, Neagu D and Irvine J T S 2013 Energy Environ. Sci. 6 256-66
- [2] Du Z, Zhao H, Yi S, Xia Q, Gong Y, Zhang Y, Cheng X, Li Y, Gu L and Świerczek K 2016 ACS Nano 10 8660-9
- [3] Madsen B D, Kobsiriphat W, Wang Y, Marks L D and Barnett S A 2007 J. Power Sources 166 64-67
- [4] Wang J et al 2021 Chem. Mater. 33 5021-34
- [5] Han H, Park J, Nam S Y, Kim K J, Choi G M, Parkin S S P, Jang H M and Irvine J T S 2019 Nat. Commun. 10 1471
- [6] Neagu D, Tsekouras G, Miller D N, Ménard H and Irvine J T S 2013 Nat. Chem. 5 916-23
- [7] Weber M L, Wilhelm M, Jin L, Breuer U, Dittmann R, Waser R, Guillon O, Lenser C and Gunkel F 2021 ACS Nano 15 4546-60
- [8] Kim K J et al 2019 J. Am. Chem. Soc. 141 7509-17
- [9] Jennings D, Ricote S, Santiso J, Caicedo J and Reimanis I 2022 Acta Mater. 228 117752
- [10] Neagu D, Oh T-S, Miller D N, Ménard H, Bukhari S M, Gamble S R, Gorte R J, Vohs J M and Irvine J T S 2015 Nat. Commun. 6 8120
- [11] Weber M L, Ma Q, Meuffels P, Hensling F V E, Lenser C, Gunkel F, Menzler N H, Dittmann R, Waser R and Guillon O 2019 ECS Trans. 91 1783–9
- [12] Kindelmann M, Stamminger M, Schön N, Rasinski M, Eichel R-A, Hausen F, Bram M and Guillon O 2021 J. Am. Ceram. Soc. 104 1465–74
- [13] Kindelmann M, Weber M L, Stamminger M, Buschhaus R, Wessel E, Bram M and Guillon O 2022 J. Eur. Ceram. Soc. 42 561–6
- [14] Istighfarini V N, Aprilia S N L and Prasetyo A 2020 IOP Conf. Ser.: Earth Environ. Sci. 456 12004
- [15] PWT 1979 J. Phys. C: Solid State Phys. 12 4977-84
- [16] Goniakowski J, Finocchi F and Noguera C 2008 Rep. Prog. Phys. 71 16501
- [17] Pojani A, Finocchi F and Noguera C 1999 Surf. Sci. 442 179-98
- [18] Wang Z, Hao X, Gerhold S, Schmid M, Franchini C and Diebold U 2014 Phys. Rev. B 90 035436
- [19] Enterkin J A, Subramanian A K, Russell B C, Castell M R, Poeppelmeier K R and Marks L D 2010 Nat. Mater. 9 245-8
- [20] Kwon O, Joo S, Choi S, Sengodan S and Kim G 2020 J. Phys. Energy 2 32001
- [21] Kim J H, Kim J K, Liu J, Curcio A, Jang J-S, Kim I-D, Ciucci F and Jung W 2021 ACS Nano 15 81–110
- [22] Gao Y, Lu Z, You T L, Wang J, Xie L, He J and Ciucci F 2018 J. Phys. Chem. Lett. 9 3772-8
- [23] de Souza R A 2009 Phys. Chem. Chem. Phys. 11 9939-69
- [24] Weber M L, Šmíd B, Breuer U, Rose M-A, Menzler N H, Dittmann R, Waser R, Guillon O, Gunkel F and Lenser C 2022 *ChemRxiv Preprint* (https://doi.org/10.26434/chemrxiv-2022-v9z6n) (Accessed 24 July 2022)
- [25] Baeumer C 2021 J. Appl. Phys. 129 170901
- [26] Kersell H, Weber M L, Falling L, Lu Q, Baeumer C, Shirato N, Rose V, Lenser C, Gunkel F and Nemšák S 2022 Faraday Discuss.
- [27] Neagu D et al 2019 ACS Nano 13 12996-3005